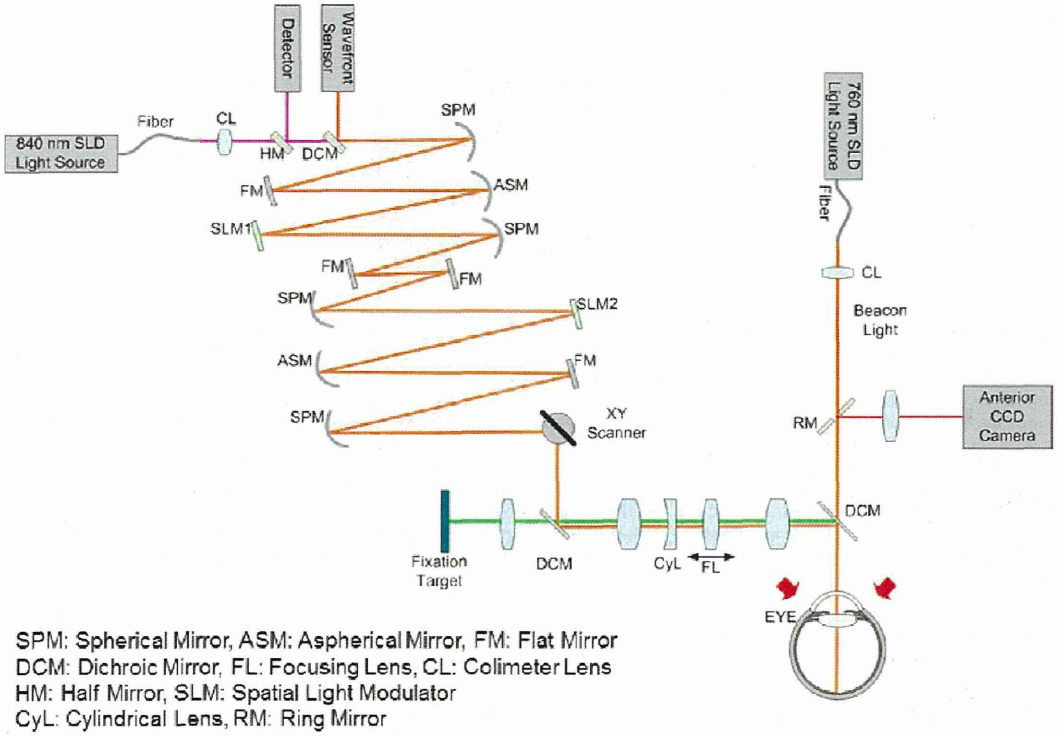

Figure 2. Schematic of the optical structure of AO-SLO. Two spatial light modulators (SLM) are used for wavefront correction, and the cylindrical lens (CyL) is used to compensate for the large astigmatism of eyes. The aspherical mirror is used to compensate for the aberration from the off-axis layout mirrors. The two *red arrows* represent the infrared light used to observe eye fixation.

processing technique for capillary visualization using AO-SLO videos.[41,42] In brief, motion contrast enhancement was conducted by dividing the pixels between sequential frames followed by calculating the variance of pixels among all division images in each X–Y position, resulting in visualization of the contrast-enhanced capillary images. Visualized vessels were used for the following analyses to set the regions of interest (ROI) along the target vessels precisely. All digital image processing for capillary visualization was manipulated by ARIA automatically.

Velocity Measurement of the Dark Tail. The target vessels with dark tail flow were selected from one branch to another to ensure that they were free of another bifurcation. The dark tail velocity was calculated by using a spatiotemporal image generated by reslicing the sequential frames, with the length of the line on the horizontal axis and the frame number on the vertical axis.[24,43] After reslicing of the frames along the line set on the target vessel (Fig. 3A), the velocity was obtained by calculating the reciprocal of the slope of the borderline between the white band and black band depicted in the spatiotemporal image, which correspond to the loci of moving bright particles and the dark tail, respectively (Fig. 3B). A steeper slope indicates a lower velocity. We measured three individual capillaries per subject, which were selected randomly. The velocities of three individual successive dark tails were measured for each capillary, yielding 90 measurements.

Measurement of Dark Tail Length. Dark tail length was calculated by using a spatiotemporal image in which the dark tail velocities and the time required for the dark tail to pass the points on the target vessel could be seen simultaneously. First, a straight vertical line was set on the spatiotemporal image and a plot profile was prepared. The frame number of the gray value range that was lower than the background gray value was measured as the time required for the dark tail to pass the point on the target vessel (Figs. 3B, 3C). The background gray value was defined as the average gray value of a region free of dark tails and bright moving objects such as leukocytes or plasma gaps. Together with the velocity of the dark tail mentioned above, the dark tail length was calculated as follows:

$$l = v \times t, \tag{1}$$

where l and v are the length and velocity of the dark tail, respectively, and t is the time required for the dark tail to pass through a point located on the target vessel. In addition, the spatiotemporal image was separated vertically into three zones from upstream to downstream of the blood flow (zones a, b, and c), and the dark tail length was calculated for each zone to evaluate time-dependent dark tail changes. The dark tail elongation rate was defined as follows:

$$r = \frac{l_c - l_a}{L}, \tag{2}$$

where r, L, l_c, and l_a are the elongation rate, the distance between zone a and zone c, the dark tail length at zone c, and the dark tail length at zone a, respectively. We measured three individual and randomly selected capillaries in each subject. The length of three individual dark tails was measured for each capillary, yielding a total of 270 measurements.

Capillary Diameter Measurement

Capillary diameters were measured to evaluate the association with the elongation rate of the dark tail. The parafoveal capillary diameters were measured on the constructed

Investigative Ophthalmology & Visual Science

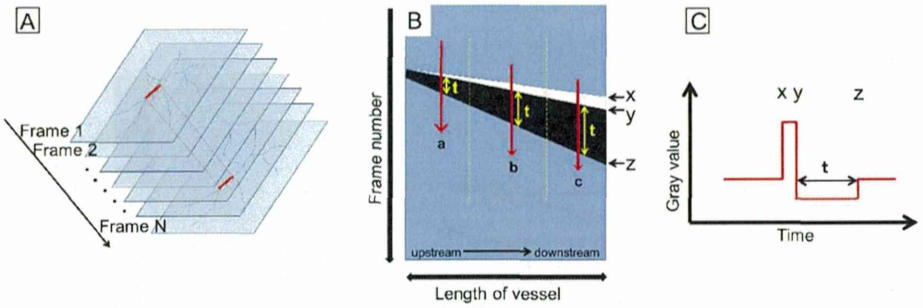

FIGURE 3. Measurement of dark tail velocity and length using a spatiotemporal image. (**A**) Schema of stacked sequential AO-SLO images. *Red lines* are focused on the target vessel in preparation for reslicing of the sequential images in order to generate the spatiotemporal image. (**B**) The dark tail velocity and length were calculated by using a spatiotemporal image that was plotted with the length of the target vessel on the horizontal axis and the frame number on the vertical axis. The *white narrow band* and the *wider black band* represent the trajectory of bright moving objects and dark tail, respectively. The thickness of the black band (t) represents the time required for the dark tail to pass through a point located on the target vessel. The reciprocal of the slope of the borderline between the white and black bands represents the velocity of the head of the dark tail. The spatiotemporal image was vertically separated into three zones from upstream to downstream of the blood flow (zones a, b, and c), and the dark tail length was calculated for each zone to evaluate the time-dependent changes in the dark tails. (**C**) Plot profile of the *red line* set on the spatiotemporal image in (**B**). Points x, y, and z and the length of time (t) correspond to x, y, z, and t in (**B**), respectively. The frame number of the gray value range that was lower than the averaged gray value was measured as the time required for the dark tail to pass the point on the target vessel. The dark tail length was computed by multiplying the velocity by the time. Dark tail velocities were calculated for each zone to evaluate the time-dependent changes in dark tails.

capillary images and were measured for each of the three zones manually.

Statistical Analysis

All values are presented as the mean ± SD. The statistically significant correlations between the elongation rate and velocity, between the elongation rate and diameter, between the velocity and diameter, and between the length of the dark tail and diameter were evaluated with the Pearson's correlation coefficient. The differences in dark tail length and capillary diameter among the three zones were evaluated with analysis of variance (ANOVA) followed by repeated measures ANOVA. All calculations were performed using StatView (version 5.0; SAS, Inc., Cary, NC) except for the intraclass correlation coefficient (ICC), which was calculated using SPSS (IBM SPSS statistics 19; IBM, Inc., Armonk, NY). *P* values less than 0.05 were considered significant.

RESULTS

Appearance of the Dark Tail

By using our prototype AO-SLO, we successfully captured bright moving objects and dark tails flowing in parafoveal capillaries in all subjects, as previously reported.[24] All dark tails were observed as black "tadpole tail"-like regions that were darker than the vessel shadow, following closely after the bright moving objects that were previously reported as leukocytes or plasma gaps (Fig. 4 and Supplementary Movie S1).[24] Although dark tails were detected in parafoveal capillaries, they were not detected in larger vessels such as the terminal artery or collecting venules. Moreover, dark tails were not detected in all of the capillaries, and they appeared to flow in a fixed path. They suddenly appeared at a branch of the parafoveal capillary, flowed in the capillary network, and disappeared when they reached the larger vessels.

Dark Tail Velocity

The average velocity of the dark tails of normal subjects was 1.49 ± 0.36 mm/s, with a range of 0.79 to 2.19 mm/s (Table).

Dark Tail Length

The lengths of the dark tails were calculated successfully in all subjects by using spatiotemporal images acquired from target vessels (Fig. 5). Examples of spatiotemporal images are shown in Figure 6. All examples show several dark bands that corresponded to the trajectories of the dark tails and were narrowest upstream and broadest downstream, indicating gradual elongation of the dark tails. The overall average length of the dark tails was 112.1 ± 36.9 μm, with a range of 21.1 to 302.2 μm. The average lengths of the dark tails at zones a, b,

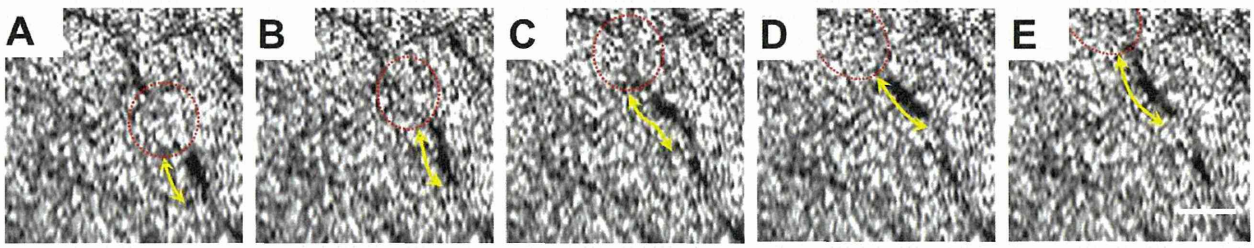

FIGURE 4. Dark tail elongation. The images show five consecutive frames with a bright particle (*dotted red circles*) and dark tail (*yellow, two-headed arrows*) flowing closely behind the bright particle in the parafoveal capillaries, which might correspond to leukocytes and erythrocyte aggregates, respectively. *Scale bar*: 100 μm. As the bright particles moved forward, the dark tails followed closely. The lengths of the dark tails became longer in a time-dependent manner, as shown by the *yellow arrows*.

Investigative Ophthalmology & Visual Science

TABLE. Characteristics of Subjects and Dark Tails

Subject	Sex	Age	Blood Pressure, mm Hg	Blood Data		Eye	Axial Length, mm	Average Velocity, mm/s	Average Dark Tail Length, μm			Average Dark Tail Elongation Rate	Average Vessel Diameter, μm
				RBC, $\times 10^4/\mu L$	Hb, g/dL				Zone a	Zone b	Zone c		
A	M	35	100/61	498	15.2	OD	26.2	1.14 ± 0.25	93.7 ± 53.5	119.7 ± 51.3	144.6 ± 42.4	0.54 ± 0.31	9.7 ± 0.3
B	F	42	98/61	415	12.7	OD	24.5	1.62 ± 0.30	61.9 ± 22.1	77.5 ± 20.0	95.3 ± 15.8	0.34 ± 0.27	8.7 ± 1.2
C	F	31	104/70	454	14.3	OD	25.1	1.48 ± 0.25	90.5 ± 20.9	144.0 ± 40.8	174.4 ± 56.5	0.54 ± 0.26	9.1 ± 0.9
D	F	23	103/64	428	13.5	OS	23.6	1.48 ± 0.28	75.7 ± 41.0	108.1 ± 42.0	135.3 ± 45.9	0.54 ± 0.22	13.0 ± 4.5
E	F	34	101/70	436	13.5	OD	24.7	1.22 ± 0.33	52.9 ± 35.2	98.7 ± 40.1	149.1 ± 47.5	0.55 ± 0.25	10.2 ± 0.4
F	M	38	107/71	500	15.5	OS	23.8	1.77 ± 0.54	86.7 ± 18.2	113.2 ± 34.2	142.1 ± 33.4	0.39 ± 0.23	10.4 ± 1.0
G	M	33	135/78	500	13.8	OD	26.3	1.58 ± 0.32	109.7 ± 35.3	150.1 ± 51.3	180.5 ± 63.5	0.74 ± 0.72	12.0 ± 0.9
H	M	40	110/64	479	14.5	OD	24.9	1.60 ± 0.34	84.1 ± 24.0	107.4 ± 23.4	135.4 ± 45.2	0.59 ± 0.56	12.2 ± 2.5
I	M	28	120/74	508	14.3	OD	27.1	1.53 ± 0.35	83.3 ± 36.8	121.3 ± 26.6	151.5 ± 32.9	0.48 ± 0.30	12.4 ± 2.0
J	F	22	102/46	522	15.7	OD	25.9	1.51 ± 0.21	73.1 ± 28.9	88.7 ± 29.1	114.2 ± 39.8	0.37 ± 0.17	11.8 ± 1.1
Mean ± SD		32.6 ± 6.7					25.2 ± 1.1	1.49 ± 0.36	81.2 ± 35.1	112.9 ± 41.4	142.2 ± 48.2	0.51 ± 0.37	11.0 ± 2.3

RBC, red blood cells; Hb, hemoglobin; OD, right eye; OS, left eye.

and c were 81.2 ± 35.1, 112.9 ± 41.4, and 142.2 ± 48.2 μm, respectively (Table). The length of the dark tails became longer in a time-dependent manner ($P < 0.0001$) (Figs. 4, 7A). The lengths of all dark tails were longer at zone c than at zone a. The overall average elongation rate was 0.51 ± 0.37, ranging from 0.02 to 1.87. Although the velocity of the dark tail was considerably slower when the length of the dark tail was longer, the elongation rate was not correlated with the velocity ($P = 0.56$, $r = -0.062$). The reproducibility of the dark tail elongation measurements was calculated by using ICC, and the obtained ICC value was 0.954.

Capillary Diameter

The mean capillary diameter in the parafovea was 11.0 ± 2.3 μm, with a range of 7.5 to 19.1. The diameters of the zones were not significantly different ($P = 0.43$) (Fig. 7B). A significant correlation was not found between diameter and velocity ($P = 0.31$, $r = 0.109$), between diameter and elongation rate ($P = 0.80$, $r = 0.027$), or between diameter and the length of the dark tail ($P = 0.15$, $r = -0.153$), suggesting that dark tail elongation was not caused by the gradual narrowing of the capillary lumen from upstream to downstream of blood flow.

DISCUSSION

In this study, we applied the AO-SLO system to monitor erythrocyte aggregates in healthy human retinas and demonstrated the phenomenon of erythrocyte aggregate elongation in the parafoveal capillaries for the first time. Careful observation of AO-SLO images revealed the pairing of a bright particle and a dark region flowing in the parafoveal capillaries (Fig. 4 and Supplementary Movie S1), which correspond to leukocytes and erythrocyte aggregates, respectively, as previously reported.[24] Their velocities and changes in length were clearly depicted in the spatiotemporal images; the dark bands, which were represented geometrically in the spatiotemporal images and corresponded to the dark tail trajectories, had a triangular or trapezoidal shape. Dark tail elongation was demonstrated by analyzing these shapes in all dark bands.

All of the dark tails showed elongation, but not shortening. Because all samples were recorded in healthy young subjects, elongation may be a physiological phenomenon that is observed normally in the human retina. Unfortunately, the mechanism of this phenomenon remains unknown because we could not finely visualize the elongating dark tail at a cellular level in the current study. However, we believe that dark tail elongation was caused by the packed erythrocytes that could not overtake the slow-moving leukocytes in the capillary lumen, thereby strongly blocking the imaging light of AO-SLO.[29] To eliminate the influence of vessel diameter difference on dark tail elongation, that is, influence on the moving object in the tapering lumen, which would be stretched and elongated, we evaluated the diameter uniformity of target vessels by dividing the vessels into thirds and measuring the diameter of each zone. The average diameter of the target vessels was 11.0 ± 2.3 μm, and significant differences were not found among the diameters of each zone ($P = 0.43$). Moreover, a significant association was not observed between the average diameter of the target vessel and the elongation rate ($P = 0.80$). These findings support the notion that dark tail elongation was not caused by the tapering lumen of vessels during the flow and that dark tail elongation would be induced by blood cell kinetics. Leukocytes might interfere with the flow of erythrocytes and induce packing of sequential erythrocytes, resulting in the detection of elongat-

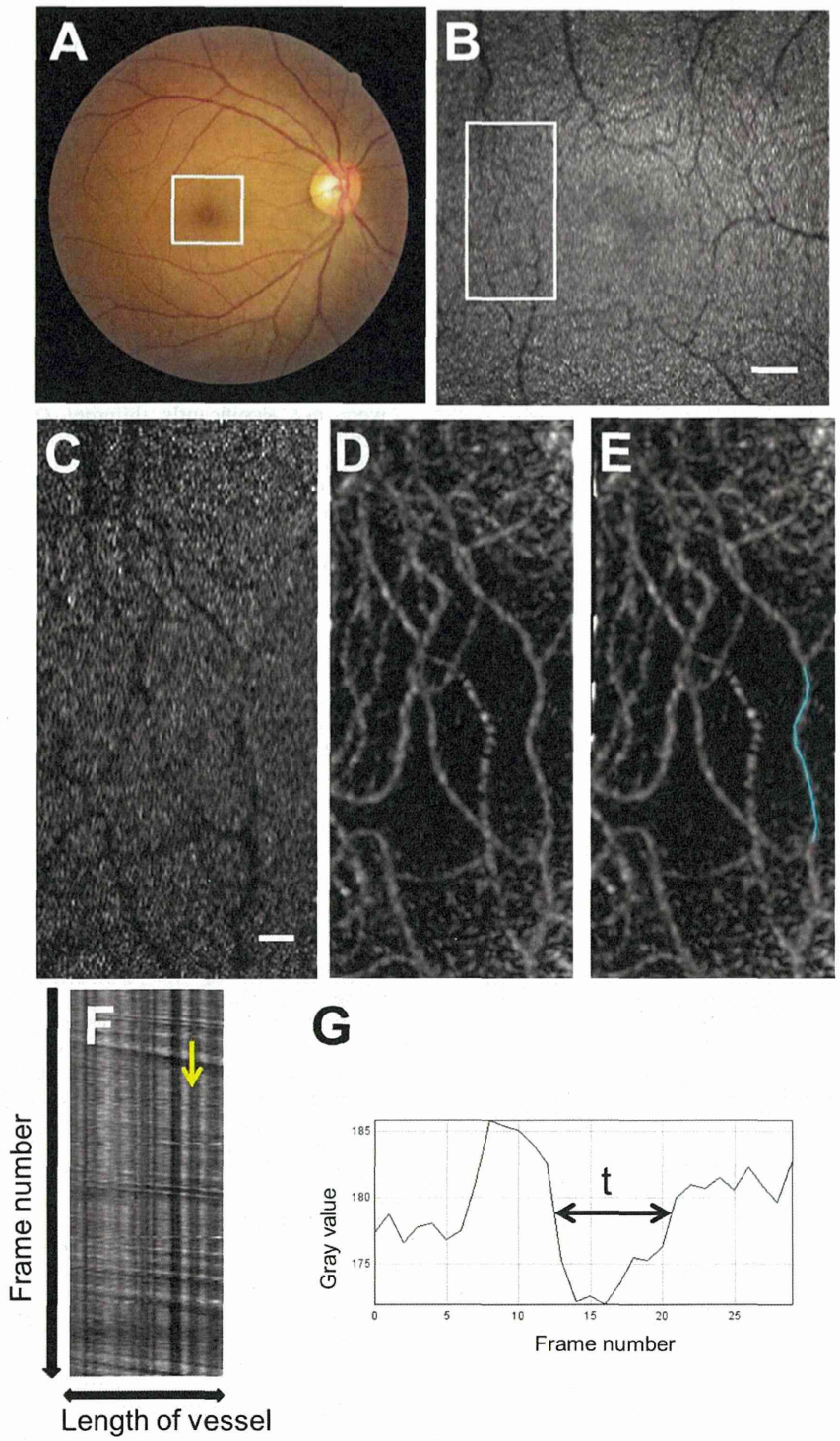

FIGURE 5. Dark tail analysis. (**A**) Color fundus photograph. (**B**) The AO-SLO image corresponds to the *outlined area* in (**A**). *Scale bar*: 200 μm. (**C**) The first frame of the AO-SLO video recorded in the *outlined area* in (**B**). *Scale bar*: 50 μm. The numerous *white dots* represent cone photoreceptors, and the *dark lines* represent the shadows of the parafoveal capillaries on the photoreceptors. (**D**) Constructed image of the capillaries. (**E**) The target vessel with dark tail flow was selected from one branch to another to ensure that they were free of another bifurcation (*blue line*). (**F**) A spatiotemporal image generated from the AO-SLO video by reslicing the frames along the line set on the target vessel (*blue line* in [**E**]) showing a white band paired with a dark band, which correspond to the trajectories of bright moving objects and dark tails, respectively. (**G**) Plot profile of the *yellow line* set on (**F**). The frame number of the gray value range that was lower than the averaged gray value (t) was measured as the time required for the dark tail to pass the point on the target vessel. The grayscale ranged from 0 (*black*) to 255 (*white*).

Investigative Ophthalmology & Visual Science

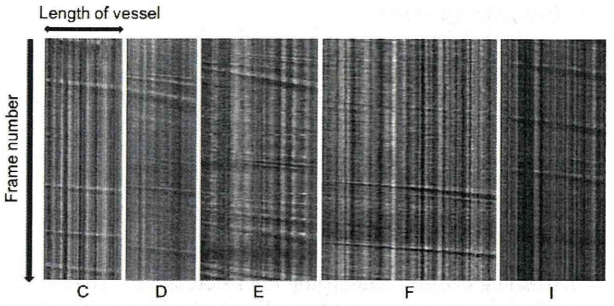

FIGURE 6. Examples of spatiotemporal images with dark tails. The letters for each image represent the subjects described in the Table. All examples show several dark bands that correspond to the trajectories of dark tails and are narrowest upstream and broadest downstream, indicating gradual elongation of dark tails.

ing dark tails closely behind the bright moving objects known as leukocytes in AO-SLO videos.[24]

It is widely accepted that erythrocytes play an extremely important role in determining the flow properties of blood.[44] Changes in the condition of erythrocytes cause impairment in microcirculation. To clarify microcirculation in diseases, erythrocyte aggregation has been used as a surrogate marker through analysis of the collected blood samples of patients. For example, increased erythrocyte aggregations were reported to be cardiovascular risk factors in patients with diabetes mellitus.[45] Erythrocyte aggregation was also increased in patients with SLE, causing a decreased flow that might contribute to the thromboembolic process.[5] In patients with Behçet's disease, increased erythrocyte aggregates are related to increased fibrinogen, but not to thrombosis and uveitis.[32] These findings motivated us to measure the dark tail velocity and the elongation of dark tail length to analyze the dynamics of erythrocyte aggregates in parafovea capillaries. Although a few studies have reported direct and noninvasive observation of erythrocyte aggregation using conjunctival blood vessels,[33] to the best of our knowledge, this is the first study to report noninvasive and direct monitoring of erythrocyte aggregates in human retinal capillaries and the phenomenon of erythrocyte aggregate elongation. In the future, the measurement of dark tail length or elongation rate will be tested in various diseases using methods that are similar to those described in this study, and their clinical importance will be investigated.

The peculiarity of AO-SLO is the correction of ocular lower- and higher-order aberrations, enabling noninvasive observation of each retinal layer, including the photoreceptor layer,[24] nerve fiber layer,[46] and capillary layer,[34] under high resolution. Although the aim of this study was to analyze blood cells, the scanning layer of AO-SLO was focused on the photoreceptor layer rather than the capillary layer, and blood cells were observed as shadings on the shadows of the bright cone mosaic patterns of photoreceptors. As previously reported, the reflected light characteristics of the AO-SLO laser from photoreceptors is affected by blood cells because of their differences in scattering coefficients.[24,47] When the scanning layer is focused on the photoreceptor layer, leukocytes are candidates for the bright particles moving in the dark vessel shadows due to the low absorptivity of the AO-SLO laser, resulting in detection of leukocytes as background illumination of photoreceptors. Blood plasma is another bright particle candidate, but its signal is slightly weaker than that of leukocytes.[24,41] Conversely, erythrocytes are strong candidates for the region that is darker than the vessel shadow because they block the AO-SLO lasers, and their aggregation is thought to be a dark tail. Because these differences in the shades on the photoreceptor layer help to distinguish blood components in the retinal microvasculature, we believe that the best focus for monitoring erythrocyte aggregation is the photoreceptor layer (Supplementary Movie S2). Meanwhile, only the numerous high-intensity particles that may correspond to a mixture of reflected light from erythrocytes and from the retinal layers near the capillary layer can be observed when the scanning layer is focused on the capillary layer, and a distinction between blood components is impossible with the accuracy of the current confocal optic system (Supplementary Movie S3).

Detection of a pair of bright particles and a dark tail flowing in the retinal circulation using AO-SLO bears a remarkable resemblance to the perception of a bright moving object and its dark tail under blue field entoptic phenomenon; this type of physiological phenomenon is perceived as numerous bright particles that move in a flowing manner with a synchronous rhythmic acceleration that corresponds to the cardiac cycle against bright, diffuse illumination.[15] Sinclair et al. suggested that leukocytes are the source of the bright particles perceived under the blue field entoptic phenomenon and that erythrocytes are detected as dark particles using animal preparations; that is, the entoptic images are the perception of the gaps between erythrocytes created by leukocytes, which have large cell bodies.[15] Erythrocyte aggregates have also been observed in retinal circulation in studies that used scanning laser ophthalmoscopy with fluorescein angiography. These studies suggested that the dark (hypofluorescent) spots detected in the stained capillaries were rouleaux formations of erythrocytes and represented erythrocyte aggregates. The fluorescein characteristics showed that the hemoglobin and oxyhemoglobin absorption bands were clearly visible in the fluorescence

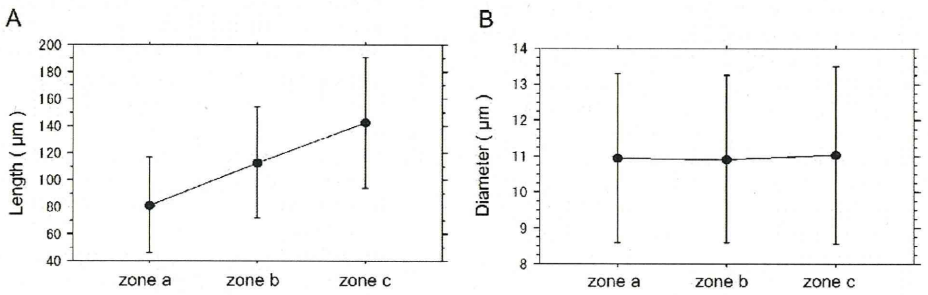

FIGURE 7. Differences in dark tail length and capillary diameter among three zones. Target vessels were separated into three zones from upstream to downstream of blood flow (zones a, b, and c) in order to evaluate the time-dependent change in dark tail length. (**A**) Significant differences in the dark tails were found among zones a, b, and c. The dark tails became longer in a time-dependent manner ($P < 0.0001$). (**B**) The diameters of the target vessels were not significantly different among the three zones ($P = 0.43$), suggesting that dark tail elongation is not caused by the gradual narrowing of the capillary lumen from upstream to downstream of blood flow.

spectra and accounted for hypofluorescent erythrocytes.[14,48,49] Unlike the above-mentioned techniques for observing erythrocyte aggregates, an approach by AO-SLO enables the analysis of erythrocyte aggregates quantitatively and without dying agents. Herein, the dark tail appearance was regarded as erythrocyte aggregates without a direct comparison of the blood components between animal preparations and AO-SLO imaging, which is a potential limitation of the current study. However, the articles described above let us speculate that the dark tail is correlated strongly with erythrocyte aggregates and that monitoring real-time changes in dark tails by AO-SLO would help us to understand the circulation physiology of the retina.

Dark tails could not be seen in vessels larger than capillaries in the current study. These large vessels were observed as dark shadows, and moving objects could not be detected in them when the scanning layer was focused on the photoreceptor layer. This can be explained by the occupation of numerous blood cells, particularly erythrocytes, in the larger vascular lumen where blood cells can easily pass through each other, preventing the imaging light of the AO-SLO from reaching the photoreceptor layer. Meanwhile, blood cells flow in single file in the capillary lumen, resulting in the detection of transparent leukocytes as bright particles and hyperreflective erythrocyte aggregates as dark shadows.[24] Moreover, dark tails could not be detected in all capillaries, and they appeared to flow in a fixed path. A possible reason for this preference is that the leukocytes, which block the current of erythrocytes through the capillary, preferred this flow path, as previously reported.[42] However, our recording time of AO-SLO was 4 seconds per one video, which is presumably too short to evaluate the flow path preference. Long-duration recording in addition to analysis of day-to-day or circadian variation of dark tail flow is required in a future study.

Given that erythrocytes cannot overtake leukocytes in the capillary lumen, it is convenient to think that the velocity of the head of the dark tail is an approximation of leukocyte velocity. In fact, the average velocity of dark tails in this study was 1.49 ± 0.36 mm/s, which is similar to the previously reported leukocyte velocities of 1.37[22] and 1.30 mm/s[35] obtained using AO-SLO. Tam et al., who first introduced spatiotemporal image analysis as a leukocyte velocity measurement, reported a faster velocity of 1.80 mm/s.[42] Although we also used spatiotemporal images to calculate the velocity of moving objects in capillaries, the velocity reported by Tam et al. was adjusted by the correction of error due to raster scan, and pulsatility was evaluated in order to calculate an accurate mean velocity, which is different from the method used herein. To improve the accuracy of velocity measurements in this study, the relationship between the direction of moving objects and the direction of the raster scan should be considered. The spatiotemporal images in this study lack slope modification to reduce the error associated with the raster scan. Although the blood dynamics in the retinal circulation require evaluations of pulsatility and raster scan error, we believe that excluding this parameter had a minimal effect on our results because our monitoring time was very short. Furthermore, our AO-SLO system can perform raster scans at 64 frames/s, which contributed to a smaller influence of raster scan error in this study. The mean error rate was calculated at 6.02% (range, 3.27%–9.11%) with reference to the formula of percent error reported by Tam et al.[50]

In conclusion, the use of AO-SLO provided a direct, noninvasive, and objective method of monitoring erythrocyte aggregates in the parafoveal capillaries of normal subjects. Erythrocyte aggregates were observed as moving dark shadows on the photoreceptor layer and became elongated in a time-dependent manner.

Acknowledgments

Supported in part by the Innovative Techno-Hub for Integrated Medical Bio-imaging Project of the Special Coordination Funds for Promoting Science and Technology from the Ministry of Education, Culture, Sports, Science and Technology (MEXT), Japan.

Disclosure: **S. Arichika**, None; **A. Uji**, None; **M. Hangai**, Canon (F, C, R); **S. Ooto**, None; **N. Yoshimura**, Canon (F, C, R)

References

1. Grading diabetic retinopathy from stereoscopic color fundus photographs—an extension of the modified Airlie House classification. ETDRS report number 10. Early Treatment Diabetic Retinopathy Study Research Group. *Ophthalmology*. 1991;98:786–806.
2. Keith NM, Wagener HP, Barker NW. Some different types of essential hypertension: their course and prognosis. *Am J Med Sci*. 1974;268:336–345.
3. Chasis H. Appreciation of the Keith, Wagener, and Barker classification of hypertensive disease. *Am J Med Sci*. 1974;268:347–351.
4. Wilkinson CP, Ferris FL III, Klein RE, et al. Proposed international clinical diabetic retinopathy and diabetic macular edema disease severity scales. *Ophthalmology*. 2003;110:1677–1682.
5. Tam J, Dhamdhere KP, Tiruveedhula P, et al. Disruption of the retinal parafoveal capillary network in type 2 diabetes before the onset of diabetic retinopathy. *Invest Ophthalmol Vis Sci*. 2011;52:9257–9266.
6. Flammer J, Orgul S, Costa VP, et al. The impact of ocular blood flow in glaucoma. *Prog Retin Eye Res*. 2002;21:359–393.
7. Sato E, Feke GT, Menke MN, Wallace McMeel J. Retinal haemodynamics in patients with age-related macular degeneration. *Eye (Lond)*. 2006;20:697–702.
8. Paques M, Garmyn V, Catier A, Naoun K, Vicaut E, Gaudric A. Analysis of retinal and choroidal circulation during central retinal vein occlusion using indocyanine green videoangiography. *Arch Ophthalmol*. 2001;119:1781–1787.
9. Spengler MI, Svetaz MJ, Leroux MB, et al. Erythrocyte aggregation in patients with systemic lupus erythematosus. *Clin Hemorheol Microcirc*. 2011;47:279–285.
10. van Heuven WA, Malik AB, Schaffer CA, Cohen D, Mehu M. Retinal blood flow derived from dye dilution curves: televised fluorescein angiography. *Arch Ophthalmol*. 1977;95:297–301.
11. Yang Y, Kim S, Kim J. Fluorescent dots in fluorescein angiography and fluorescein leukocyte angiography using a scanning laser ophthalmoscope in humans. *Ophthalmology*. 1997;104:1670–1676.
12. Paques M, Boval B, Richard S, et al. Evaluation of fluorescein-labeled autologous leukocytes for examination of retinal circulation in humans. *Curr Eye Res*. 2000;21:560–565.
13. Riva CE, Petrig B. Blue field entoptic phenomenon and blood velocity in the retinal capillaries. *J Opt Soc Am*. 1980;70:1234–1238.
14. Arend O, Harris A, Sponsel WE, Remky A, Reim M, Wolf S. Macular capillary particle velocities: a blue field and scanning laser comparison. *Graefes Arch Clin Exp Ophthalmol*. 1995;233:244–249.
15. Sinclair SH, Azar-Cavanagh M, Soper KA, Tuma RF, Mayrovitz HN. Investigation of the source of the blue field entoptic phenomenon. *Invest Ophthalmol Vis Sci*. 1989;30:668–673.
16. Sato E, Nagaoka T, Yokota H, Takahashi A, Yoshida A. Correlation between plasma pentosidine concentrations and retinal hemodynamics in patients with type 2 diabetes. *Am J Ophthalmol*. 2012;153:903–909, e901.

Investigative Ophthalmology & Visual Science

17. Riva CE, Geiser M, Petrig BL. Ocular blood flow assessment using continuous laser Doppler flowmetry. *Acta Ophthalmol.* 2010;88:622–629.
18. Riva CE, Grunwald JE, Sinclair SH, Petrig BL. Blood velocity and volumetric flow rate in human retinal vessels. *Invest Ophthalmol Vis Sci.* 1985;26:1124–1132.
19. Yoshida A, Feke GT, Mori F, et al. Reproducibility and clinical application of a newly developed stabilized retinal laser Doppler instrument. *Am J Ophthalmol.* 2003;135:356–361.
20. Nagahara M, Tamaki Y, Tomidokoro A, Araie M. In vivo measurement of blood velocity in human major retinal vessels using the laser speckle method. *Invest Ophthalmol Vis Sci.* 2011;52:87–92.
21. Kim DY, Fingler J, Zawadzki RJ, et al. Noninvasive imaging of the foveal avascular zone with high-speed, phase-variance optical coherence tomography. *Invest Ophthalmol Vis Sci.* 2012;53:85–92.
22. Martin JA, Roorda A. Direct and noninvasive assessment of parafoveal capillary leukocyte velocity. *Ophthalmology.* 2005; 112:2219–2224.
23. Zhong Z, Song H, Chui TY, Petrig BL, Burns SA. Noninvasive measurements and analysis of blood velocity profiles in human retinal vessels. *Invest Ophthalmol Vis Sci.* 2011;52:4151–4157.
24. Uji A, Hangai M, Ooto S, et al. The source of moving particles in parafoveal capillaries detected by adaptive optics scanning laser ophthalmoscopy. *Invest Ophthalmol Vis Sci.* 2012;53: 171–178.
25. Zhong Z, Petrig BL, Qi X, Burns SA. In vivo measurement of erythrocyte velocity and retinal blood flow using adaptive optics scanning laser ophthalmoscopy. *Opt Express.* 2008;16: 12746–12756.
26. Ye T, Li H, Lam KY. Modeling and simulation of microfluid effects on deformation behavior of a red blood cell in a capillary. *Microvasc Res.* 2010;80:453–463.
27. Korin N, Bransky A, Dinnar U. Theoretical model and experimental study of red blood cell (RBC) deformation in microchannels. *J Biomech.* 2007;40:2088–2095.
28. Jeong JH, Sugii Y, Minamiyama M, Okamoto K. Measurement of RBC deformation and velocity in capillaries in vivo. *Microvasc Res.* 2006;71:212–217.
29. Schmid-Schonbein GW, Usami S, Skalak R, Chien S. The interaction of leukocytes and erythrocytes in capillary and postcapillary vessels. *Microvasc Res.* 1980;19:45–70.
30. Lei H, Karniadakis GE. Quantifying the rheological and hemodynamic characteristics of sickle cell anemia. *Biophys J.* 2012;102:185–194.
31. Tsukada K, Sekizuka E, Oshio C, Minamitani H. Direct measurement of erythrocyte deformability in diabetes mellitus with a transparent microchannel capillary model and high-speed video camera system. *Microvasc Res.* 2001;61:231–239.
32. Ricart JM, Vaya A, Todoli J, Santaolaria ML, Calvo J, Aznar J. Erythrocyte aggregation in Behcet's disease determined with the Sefam and Myrenne aggregometer. Lack of association with thrombosis and uveitis. *Clin Hemorheol Microcirc.* 2005;33: 389–396.
33. Jung F, Korber N, Kiesewetter H, Prunte C, Wolf S, Reim M. Measuring the microcirculation in the human conjunctiva bulbi under normal and hyperperfusion conditions. *Graefes Arch Clin Exp Ophthalmol.* 1983;220:294–297.
34. Roorda A, Romero-Borja F, Donnelly W III, Queener H, Hebert T, Campbell M. Adaptive optics scanning laser ophthalmoscopy. *Opt Express.* 2002;10:405–412.
35. Martin JA, Roorda A. Pulsatility of parafoveal capillary leukocytes. *Exp Eye Res.* 2009;88:356–360.
36. Hofer H, Artal P, Singer B, Aragon JL, Williams DR. Dynamics of the eye's wave aberration. *J Opt Soc Am A Opt Image Sci Vis.* 2001;18:497–506.
37. Burns SA, Tumbar R, Elsner AE, Ferguson D, Hammer DX. Large-field-of-view, modular, stabilized, adaptive-optics-based scanning laser ophthalmoscope. *J Opt Soc Am A Opt Image Sci Vis.* 2007;24:1313–1326.
38. Hirose F, Nozato K, Saito K, Numajiri Y. A compact adaptive optics scanning laser ophthalmoscope with high-efficiency wavefront correction using dual liquid crystal on silicon - spatial light modulator. *Proc SPIE.* 2011;5:7885.
39. Lasers ANSftSUo. *American National Standard for the Safe Use of Lasers.* ANSI Z136.1-2007. American National Standards Institute; 2007.
40. George W. *Digital Image Warping.* Los Alamitos, CA: IEEE Computer Society Press; 1990:187–260.
41. Tam J, Martin JA, Roorda A. Noninvasive visualization and analysis of parafoveal capillaries in humans. *Invest Ophthalmol Vis Sci.* 2010;51:1691–1698.
42. Tam J, Tiruveedhula P, Roorda A. Characterization of single-file flow through human retinal parafoveal capillaries using an adaptive optics scanning laser ophthalmoscope. *Biomed Opt Express.* 2011;2:781–793.
43. Sato Y, Chen J, Yamamoto S, et al. Measuring microcirculation using spatiotemporal image analysis. *Lecture Notes in Computer Science.* 1995;302–308.
44. Chien S, Jan K. Ultrastructural basis of the mechanism of rouleaux formation. *Microvasc Res.* 1973;5:155–166.
45. MacRury SM, Lennie SE, McColl P, Balendra R, MacCuish AC, Lowe GD. Increased red cell aggregation in diabetes mellitus: association with cardiovascular risk factors. *Diabet Med.* 1993; 10:21–26.
46. Takayama K, Ooto S, Hangai M, et al. High-resolution imaging of the retinal nerve fiber layer in normal eyes using adaptive optics scanning laser ophthalmoscopy. *PLoS One.* 2012;7: e33158.
47. Meinke M, Muller G, Helfmann J, Friebel M. Optical properties of platelets and blood plasma and their influence on the optical behavior of whole blood in the visible to near infrared wavelength range. *J Biomed Opt.* 2007;12:014024.
48. Arend O, Harris A, Wolf S. Capillary blood flow velocity measurements in cystoid macular edema with the scanning laser ophthalmoscope. *Am J Ophthalmol.* 1994;117:819–820.
49. Ohnishi Y, Fujisawa K, Ishibashi T, Kojima H. Capillary blood flow velocity measurements in cystoid macular edema with the scanning laser ophthalmoscope. *Am J Ophthalmol.* 1994; 117:24–29.
50. Tam J, Roorda A. Speed quantification and tracking of moving objects in adaptive optics scanning laser ophthalmoscopy. *J Biomed Opt.* 2011;16:036002.

Investigative Ophthalmology & Visual Science

OPEN ACCESS Freely available online

PLOS ONE

Adaptive Optics-Assisted Identification of Preferential Erythrocyte Aggregate Pathways in the Human Retinal Microvasculature

Shigeta Arichika, Akihito Uji*, Sotaro Ooto, Kazuaki Miyamoto, Nagahisa Yoshimura

Department of Ophthalmology and Visual Sciences, Kyoto University Graduate School of Medicine, Kyoto, Japan

Abstract

Purpose: To characterize human parafoveal blood flow using adaptive optics scanning laser ophthalmoscopy (AO-SLO).

Methods: In 5 normal subjects, erythrocyte aggregate distributions were analyzed on 3 different days. Erythrocyte aggregates were described as a "dark tail" in AO-SLO. The characteristics of the pathways with dark tail flow in the parafovea were measured. Additionally, the tendency for dark tail flow before and after bifurcations was analyzed to study the blood flow in detail.

Results: Average velocity in parent vessels with dark tail flow was 1.30±0.27 mm/s. Average velocity in daughter vessels with dark tail flow was 1.12±0.25 mm/s, and the average velocity of plasma gaps in daughter vessels without dark tail flow was 0.64±0.11 mm/s. Downstream from the bifurcations, the velocity in vessels with dark tail flow was higher than that in those without it ($p<0.001$), and the branching angles of vessels with dark tail flow were smaller than those of vessels without it ($p<0.001$).

Conclusions: Images from the AO-SLO noninvasively revealed pathways with and without dark tail flow in the human parafovea. Pathways with dark tail flow in the daughter vessels generally had faster flow and smaller bifurcation angles than daughter vessels without dark tail flow. Thus, AO-SLO is an instructive tool for analyzing retinal microcirculatory hemodynamics.

Citation: Arichika S, Uji A, Ooto S, Miyamoto K, Yoshimura N (2014) Adaptive Optics-Assisted Identification of Preferential Erythrocyte Aggregate Pathways in the Human Retinal Microvasculature. PLoS ONE 9(2): e89679. doi:10.1371/journal.pone.0089679

Editor: Anand Swaroop, National Eye Institute, United States of America

Received December 2, 2013; **Accepted** January 21, 2014; **Published** February 26, 2014

Funding: This study was supported in part by the Innovative Techno-Hub for Integrated Medical Bioimaging of the Project for Developing Innovation Systems, from the Ministry of Education, Culture, Sports, Science and Technology (MEXT), Japan. No additional external funding received for this study. The funders had no role in study design, data collection and analysis, decision to publish, or preparation of the manuscript.

Competing Interests: This study was supported in part by Canon Inc. Canon Inc. has provided a prototype of AO-SLO system to the authors' institution. This does not alter the authors' adherence to all the PLOS ONE policies on sharing data and materials.

* E-mail: akihito1@kuhp.kyoto-u.ac.jp

Introduction

Ophthalmoscopy is a standard procedure in every routine eye examination and is useful in detecting retinal changes caused directly by eye disease and those secondary to systemic disease. This includes retinal blood vessel changes resulting from high blood pressure [1,2,3], arteriosclerosis [4], and diabetes mellitus. [5] Detecting the earliest visible signs of diabetic retinopathy (e.g., microaneurysms and dot hemorrhages) or staging systemic hypertensive and arteriosclerotic changes (using the Keith-Wagener [3] and Scheie [4] classification systems) are important in preventing systemic disease processes.

In addition to ophthalmoscopic examination, other approaches have been used to analyze the retinal circulation in more detail. Fluorescein angiography (FA) has long been the prevalent technique and the gold standard for evaluating retinal circulation, even with the potential side effects of fluorescein and the discomfort associated with the procedure. These drawbacks may prevent normal subjects and patients with early disease from undergoing angiography. Therefore, other tools that do not rely on an angiographic agent for measuring retinal blood flow have been developed, including laser Doppler velocimetry [6], scanning laser Doppler flowmetry [7], laser speckle flowmetry [8], and retinal functional imager. [9] Additionally, improved optical coherence tomography (OCT) systems, such as the Doppler OCT [10], can be used to examine retinal hemodynamics without a contrast agent.

Nishiwaki et al. [11,12], Miyamoto et al. [13], and Kimura et al. [14] evaluated the animal retinal microcirculation using acridine orange and a scanning laser ophthalmoscope (SLO) system. Interestingly, they reported that leukocytes, when faced with a bifurcation, preferentially distribute themselves into the branch with the higher flow rate. [12] They concluded that these preferential pathways had a lower resistance and protected the retina by preventing leukocytes from entering small capillaries, where they would likely plug the small vessels. Unfortunately, acridine orange is toxic and cannot be used to study this phenomenon in humans.

Adaptive optics (AO) ophthalmoscopy was recently developed and has the ability to visualize photoreceptors [15,16] and

evaluate the retinal nerve fiber bundle [17] retinal blood flow [18,19,20], blood corpuscles [21,22], and retinal vasculature [23] Cells visualized with adaptive optics scanning laser ophthalmoscopy (AO-SLO) included leukocytes, erythrocyte aggregates, and plasma gaps, and the visualization was achieved with a noninvasive, objective, agent-free approach. Specifically, AO-SLO [18,19,24,25,26,27] was used to measure blood velocity in larger vessels [27] and leukocyte velocity in the parafovea. [19,28] It was also used to noninvasively characterize plasma gaps and single-file flow of leukocytes [18] in humans. We previously reported bright particles moving in capillaries, which we suspect may be reflections of the photoreceptor, visible when circulating transparent objects (e.g., leukocytes or plasma gaps) pass over the photoreceptor. We also described the "dark tail," which we interpreted as a region darker than the vessel shadow, that may correspond to aggregated erythrocytes upstream of leukocytes. Interestingly, the dark tail elongated in a time-dependent manner. [22] Erythrocyte aggregates are considered to be an important hemorheological determinant of microcirculatory problems [29,30,31] and an important hemorheological parameter because of their direct effects on whole blood viscosity. [32] Thus, direct monitoring of retinal erythrocyte aggregates in patients may provide early indications not visible on ophthalmoscopy of a microcirculatory disorder.

Here, we use the AO-SLO to examine erythrocyte aggregate (dark tail) distribution in the retinal capillary network in humans. We also analyze flow preferences of these dark tails in the parafovea.

Methods

This study was approved by the Institutional Review Board and the Ethics Committee at Kyoto University Graduate School of Medicine. The study conduct adhered to the tenets of the Declaration of Helsinki. Written informed consent was obtained from each participant after the nature of the study and the risks and benefits of study participation were thoroughly explained.

Subjects

Videos of the parafoveal areas were acquired using AO-SLO in 5 healthy Japanese subjects. All subjects had a medical history free of ocular and systemic disease. The eyes of all subjects were dilated before AO-SLO image acquisition with 1 drop each of tropicamide (0.5%) and phenylephrine hydrochloride (0.5%). Following dilation, subjects were examined for approximately 20 minutes per eye in a seated posture. All subjects had normal ophthalmoscopic findings, blood pressure, and intraocular pressure (IOP). Subject B in this paper also served as subject A in a previous report. [22] All AO-SLO images were acquired specifically for this study. All subjects underwent AO-SLO imaging three times, with each examination separated by an interval of at least one week. This was done to ensure that dark tail measurements were reproducible in terms of distribution and flow direction. Each vessel was imaged for at least 30 seconds.

Adaptive Optics Scanning Laser Ophthalmoscope Imaging

We developed a novel AO-SLO system (Canon Inc., Tokyo, Japan) with a high wavefront correction efficiency by using a dual liquid-crystal phase modulator (LCOS-SLM; X10468-02, Hamamatsu, Japan). [21,22] The AO-SLO videos were acquired at 32 or 64 frames/s in the area covering the parafovea. The scan area was $2.8^\circ \times 2.8^\circ$ or $1.4^\circ \times 2.8^\circ$ at the retina and had a sampling of 400×400 or 200×400 pixels, respectively. Velocities of moving objects in vessel shadows were analyzed at a rate of 64 frames/s. All AO-SLO imaging procedures were performed with the optical focus on the photoreceptor layer. [22].

Detection and Measurement of Dark Tail

We investigated the shadows of aggregated erythrocytes that block the AO-SLO laser, creating a "dark tail." The dark tail was defined as a dark region (darker than the vessel shadow) that occurred closely behind a bright, moving particle within a vessel (Figure 1).

A montage of the parafoveal capillary network was manually created by overlapping constructed capillary projections (Figure 2A). Capillary images were constructed as projections of moving objects in sequential frames by using the motion contrast-enhancement technique [18,25], which utilizes the AO-SLO Retinal Image Analyzer (ARIA, Canon Inc., Tokyo, Japan). [22] From these sequential frames, the foveal avascular zone (FAZ) boundary was manually determined. The region of interest (ROI) was automatically generated based on the FAZ boundary, according to the methods described by Tam et al. [25] The distance transform was then used to calculate how far pixels were outside of the FAZ boundary. Pixels inside of the FAZ and further than 150 μm from the edge of the FAZ were excluded from analyses (Figure 2B). This annulus surrounding the FAZ was regarded as a capillary monolayer in the human macula. [25].

In order to analyze dark tail distributions, we separated blood flow within the analytic region into pathways with dark tail flow and pathways without dark tail flow. The distinction between dark tail and non-dark tail flow was made through careful observation and analysis of AO-SLO movies and corresponding spatiotemporal (ST) images (Figure 3B). The length of the whole pathway was manually measured in both types of pathways, as well as the length along the FAZ boundary.

Characterization of Blood Flow and Vessel Patterns at Bifurcations

Bifurcations consisting of a parent vessel with a dark tail flow, a daughter vessel with a dark tail flow, and a daughter vessel without a dark tail flow were chosen to analyze factors determining dark tail preferential pathways. Blood components were identified using ST images, according to the methods described by Tam et al. [18] Briefly, leukocyte traces were identified as (i) thick, (ii) high contrast, (iii) sparse, or (iv) unidirectional (Figure 3B). Plasma gap traces, which tended to have lower contrast than leukocyte traces, were identified as (i) thin or (ii) dense (Figure 3C). Dark tail traces following leukocyte traces were identified as (i) thick, (ii) high contrast, or (iii) hyporeflective (Figure 3B). [22].

Blood flow velocity measurement at bifurcations. All bifurcation images with sufficient quality were used to detect moving blood components, including dark tails, leukocytes, and plasma. At bifurcations, the dark tail flow in the parent vessel was bisected into dark tail flow and dark tail-free flow in the daughter vessels. The difference in blood flow velocity between the daughter vessel with and without a dark tail flow was determined by comparing dark tail velocity in the dark tail daughter vessel and plasma velocity in the non-dark tail daughter vessel. This method has been described in full in another study. [22] Briefly, sequential frames of the same vessel were compared, placing the length of the line on the horizontal axis and the frame number on the vertical axis. A white band, black band, and white line corresponded to the trajectories of moving leukocytes, dark tails (Figure 3B), and plasma gaps (Figure 3C), respectively. Dark tail and plasma gap velocities were obtained by calculating the reciprocal of the slope of the borderline between the white and black bands and the white

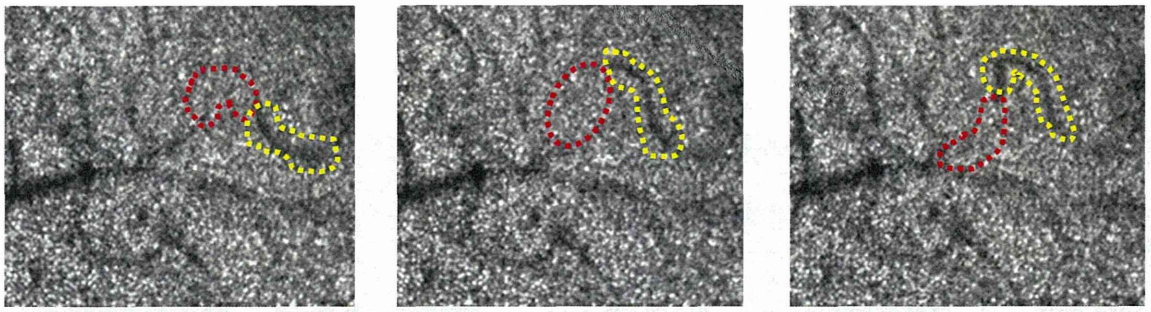

Figure 1. Consecutive AO-SLO images from a normal subject. Bright particles and dark regions were identified in vessel shadows on the cone mosaic. Bright particles are thought to represent leukocytes and plasma gaps. Dark regions represent erythrocyte aggregates, described as a "dark tail." The red dot circles and yellow dot circles highlight bright particles and dark tails, respectively. Blood flow direction was from the right to the left side.
doi:10.1371/journal.pone.0089679.g001

line depicted in the ST image. In order to synchronize the velocity and the cardiac cycle, a pulse oximeter (Oxypal Neo, NIHON KOHDEN, Japan) was attached to the subject's earlobe. As was done by Martin et al. [19], measurements were divided into five equal bins, each corresponding to the segment of the cardiac cycle in which they were observed. [19] To correct for the influence of the cardiac cycle on measured velocities, the average velocity during each of the 5 cardiac cycle segments was calculated separately. The total average velocity was then calculated by averaging each cycle segment velocity.

Measurement of capillary diameter. The diameters of 3 capillaries (1 parent and 2 daughter vessels) were measured at each bifurcation by using the constructed capillary images. [22] Values were then analyzed to determine the influence of vessel diameter on dark tail pathway preference. For each vessel, average diameter was manually calculated by taking measurements 10, 20, and 30 μm from the bifurcation. For each subject, diameters of 4 bifurcations were analyzed, yielding measurements for 20 bifurcations and 60 vessels.

Measuring angles between parent and daughter vessels. Angles between parent and daughter vessels were measured to determine the influence of angles on dark tail pathway preference. Measurements were made with the assistance of public-domain image analysis software (ImageJ, National Institutes of Health, Bethesda, MD). The standard line for measuring angles was drawn by joining the midpoints of the diameter of the parent vessel, which were determined at two points–at the center of the bifurcation and at a point 50 μm upstream of the bifurcation. Next, straight lines were drawn on the 2 daughter vessels in the same fashion. Lastly, angles between the extended parent vessel and each daughter vessel were measured. For each subject, 4 bifurcations were analyzed, yielding a study total of 20 bifurcations and 40 angles.

Statistical Analyses

All values are presented as mean ± standard deviation (SD). Paired *t*-tests were used to examine the statistical significance of differences between dark tail and non-dark tail pathway length in the region 150 μm away from the FAZ, dark tail and non-dark tail pathway separations on the FAZ boundary, and the angle between daughter vessels in bifurcations. Comparisons of velocities and vessel diameters of the 3 vessels (1 parent and 2 daughter vessels) were carried out using repeated measures analysis of variance, and differences between the 2 groups were analyzed using the paired *t*-test, followed by Bonferroni correction. All calculations were

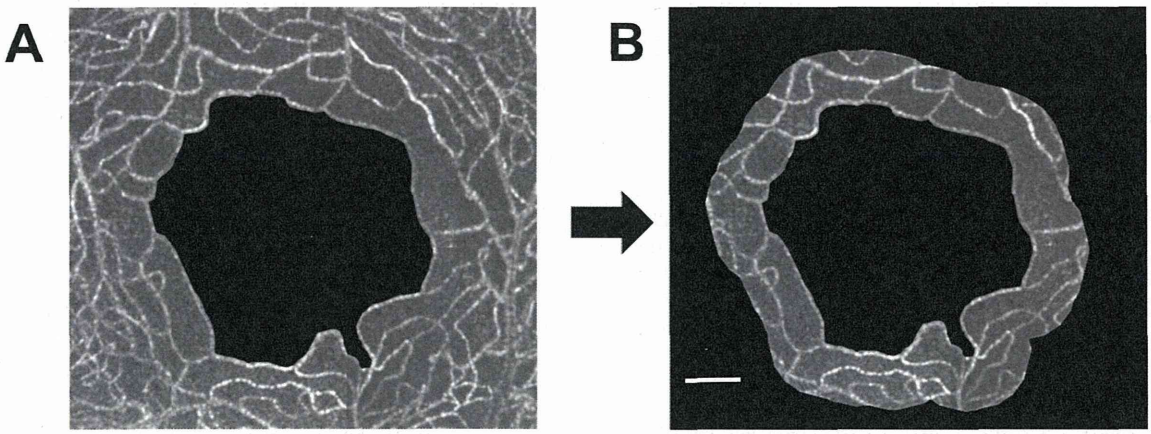

Figure 2. Extraction of parafoveal network data. (A) Montage of the parafoveal capillary network. The center black region represents the foveal avascular zone (FAZ). (B) Doughnut-shaped region within 150 μm of the FAZ edge. Vessel lengths were measured within the doughnut-shaped region and on the border of the FAZ. Scale bar represents 150 μm.
doi:10.1371/journal.pone.0089679.g002